

A *de novo* gain-of-function mutation in *SCN11A* causes loss of pain perception

Enrico Leipold¹, Lutz Liebmann², G Christoph Korenke³, Theresa Heinrich², Sebastian Gießelmann², Jonathan Baets^{4–6}, Matthias Ebbinghaus⁷, R Oliver Goral¹, Tommy Stödtberg⁸, J Christopher Hennings², Markus Bergmann⁹, Janine Altmüller¹⁰, Holger Thiele¹⁰, Andrea Wetzel¹¹, Peter Nürnberg^{10,12–14}, Vincent Timmerman^{4,15}, Peter De Jonghe^{4–6}, Robert Blum¹¹, Hans-Georg Schaible⁷, Joachim Weis¹⁶, Stefan H Heinemann¹, Christian A Hübner² & Ingo Kurth²

The sensation of pain protects the body from serious injury^{1–3}. Using exome sequencing, we identified a specific *de novo* missense mutation in *SCN11A* in individuals with the congenital inability to experience pain who suffer from recurrent tissue damage and severe mutilations. Heterozygous knock-in mice carrying the orthologous mutation showed reduced sensitivity to pain and self-inflicted tissue lesions, recapitulating aspects of the human phenotype. *SCN11A* encodes Na_v1.9, a voltage-gated sodium ion channel that is primarily expressed in nociceptors, which function as key relay stations for the electrical transmission of pain signals from the periphery to the central nervous system^{4,5}. Mutant Na_v1.9 channels displayed excessive activity at resting voltages, causing sustained depolarization of nociceptors, impaired generation of action potentials and aberrant synaptic transmission. The gain-of-function mechanism that underlies this channelopathy suggests an alternative way to modulate pain perception.

Pain stimuli are detected by nociceptors—neurons that transmit sensory information via long axons from the body periphery to the spinal cord⁶. A diminished pain response can be caused by degeneration of these neurons or by impaired electric signaling. In either case, a lack of protective behavior toward noxious stimuli predisposes to fractures, burns and mutilations.

Disorders accompanied by neuronal loss are classified as hereditary sensory and autonomic neuropathies (HSANs). They involve genes that are crucial for sphingolipid metabolism, neurotrophin action, axonal transport, DNA methylation and membrane shaping

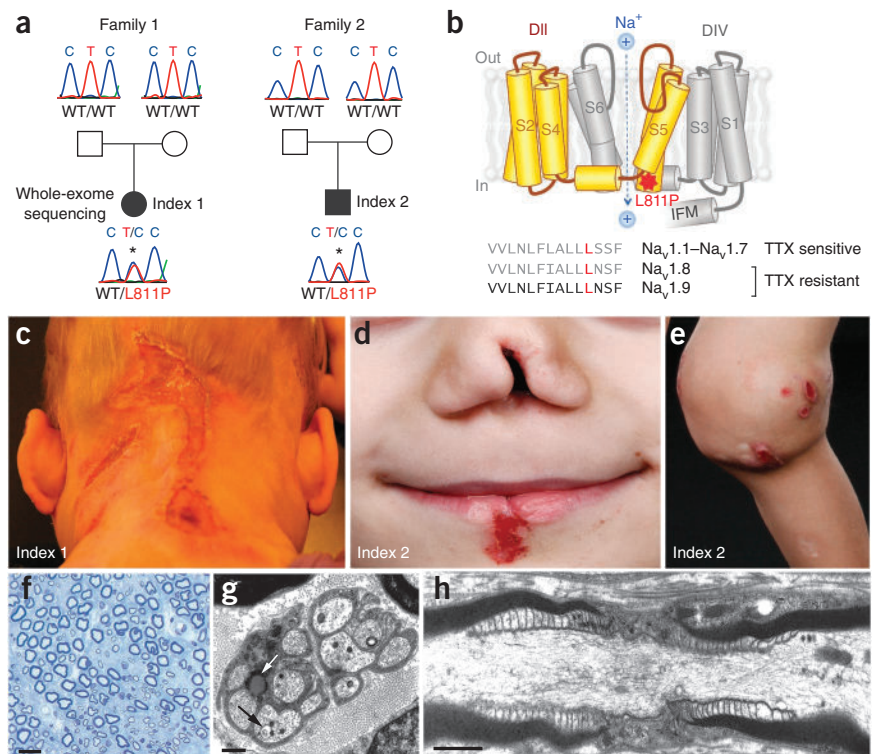
of organelles^{7,8}. Nociceptor function also depends on voltage-gated sodium ion (Na_v) channels that are essential for the generation of action potentials. Biallelic loss-of-function mutations in *SCN9A*, encoding sodium ion channel Na_v1.7, have been shown to cause an inability to experience pain by impairing the electrical signaling of morphologically intact axons⁹. However, null alleles of *SCN9A* have recently been reported in individuals with loss of large sensory fibers, suggesting that neurodegeneration and lack of ion channel activity are not mutually exclusive¹⁰.

To identify determinants of pain perception, we performed whole-exome sequencing of a German trio of healthy parents and their daughter diagnosed with the congenital inability to experience pain (index subject 1). We mapped reads to the human genome reference build hg19 using the Burrows-Wheeler (BWA) alignment algorithm¹¹ and performed *de novo* single-nucleotide variant (SNV) and short indel calling using the family-aware Illumina genotype likelihood-based method (FIGL)¹². Filtering for autosomal variants not present in dbSNP135, the 1000 Genomes Project database and the Exome Variant Server resulted in the identification of 472 rare variants in 440 genes. A heterozygous nonsynonymous mutation c.2432T>C (p.Leu811Pro) in exon 15 of the *SCN11A* gene was identified as the only *de novo* event in index subject 1 (Fig. 1a). As the average rate of *de novo* mutations per exome and generation is only 0 to 1 (ref. 13), we considered this variant to be particularly disease relevant¹⁴. *SCN11A* encodes the voltage-gated sodium ion channel Na_v1.9, which is highly expressed in nociceptors¹⁵. The mutation results in the replacement of leucine 811 by proline at the distal end of the sixth transmembrane segment in domain II of Na_v1.9, a position that is highly conserved in mammals and among the nine human Na_v channels (Fig. 1b).

¹Center for Molecular Biomedicine, Department of Biophysics, Friedrich Schiller University Jena and Jena University Hospital, Jena, Germany. ²Institute of Human Genetics, Jena University Hospital, Jena, Germany. ³Department of Neuropediatrics, Pediatric Center, Oldenburg Hospital, Oldenburg, Germany. ⁴Neurogenetics Laboratory, Institute Born-Bunge, University of Antwerp, Antwerp, Belgium. ⁵Neurogenetics Group, Department of Molecular Genetics, VIB, University of Antwerp, Antwerp, Belgium. ⁶Department of Neurology, Antwerp University Hospital, Antwerp, Belgium. ⁷Institute of Physiology, Division of Neurophysiology, Jena University Hospital, Jena, Germany. ⁸Department of Neuropediatrics, Karolinska University Hospital, Stockholm, Sweden. ⁹Institute for Neuropathology, Hospital Bremen-Mitte, Bremen, Germany. ¹⁰Cologne Center for Genomics (CCG), University of Cologne, Cologne, Germany. ¹¹Institute for Clinical Neurobiology, University of Würzburg, Würzburg, Germany. ¹²Cologne Excellence Cluster on Cellular Stress Responses in Aging-Associated Diseases (CECAD), University of Cologne, Cologne, Germany. ¹³ATLAS Biolabs, Berlin, Germany. ¹⁴Center for Molecular Medicine Cologne (CMCC), University of Cologne, Cologne, Germany. ¹⁵Peripheral Neuropathy Group, Department of Molecular Genetics, VIB, University of Antwerp, Antwerp, Belgium. ¹⁶Institute of Neuropathology, RWTH Aachen University Hospital and Jülich Aachen Research Alliance (JARA) Brain Translational Medicine, Aachen, Germany. Correspondence should be addressed to I.K. (ingo.kurth@med.uni-jena.de).

Received 22 May; accepted 26 August; published online 15 September 2013; doi:10.1038/ng.2767

Figure 1 An *SCN11A* mutation results in the inability to experience pain in humans. (a) A *de novo* heterozygous mutation in *SCN11A* (c.2432T>C; p.Leu811Pro; indicated by asterisk) was identified by exome sequencing of index subject 1. Sequencing of the *SCN11A* gene identified the same *de novo* mutation in an additional subject with the inability to experience pain (index subject 2). (b) Schematic of domain II (DII) and domain IV (DIV) of the Na_v1.9 α subunit, encoded by *SCN11A*; domains I and III are not depicted for clarity. The red asterisk marks the position of the p.Leu811Pro alteration on the intracellular face of the channel; this structure also interacts with a conserved IFM motif, which mediates rapid channel inactivation. Bottom, alignment of protein sequences at the end of segment S6 in DII from all human voltage-gated sodium channels (Na_v1.1–Na_v1.9) with the leucine residue of interest (Leu811 in Na_v1.9) highlighted in red. TTX, tetrodotoxin. (c) Painless tissue damage in index subject 1 due to the inability to experience pain. (d) Nose and lip wounds of index subject 2. (e) Malposition of the knee joint resulted from repeated painless fractures. (f) Sural-nerve biopsy of index subject 1 showed a normal density of large and small myelinated nerve fibers. Semithin section, toluidine blue stain. Scale bar, 30 μ m. (g) Electron microscopy images showing only minor, nonspecific alterations of unmyelinated nerve fibers. Autophagic vesicles were observed in axons (black arrow), similar to lipofuscin-like aggregates in the non-myelinating Schwann cells of Remak bundles (white arrow). Scale bar, 0.8 μ m. (h) Normal ultrastructure of a node of Ranvier. Scale bar, 0.5 μ m.



To corroborate a role for *SCN11A* in human pain perception, we performed Sanger sequencing of *SCN11A* exons in 58 independent individuals with early-onset severe sensory loss, of whom 52 represented sporadic cases. In a Swedish male (index subject 2), we identified exactly the same heterozygous *SCN11A* mutation, again as a *de novo* event (Fig. 1a). The clinical history of both affected individuals was remarkably similar, involving a congenital inability to experience pain since birth resulting in self-mutilations, slow-healing wounds and multiple painless fractures (Fig. 1c–e). Both individuals presented with mild muscular weakness and delayed motor development. Muscle biopsy and electromyography (EMG) were normal. Electroneurography showed slightly reduced motor and sensory nerve conduction velocities with normal amplitudes. Investigations of nerves by sural biopsy in index subject 1 did not show sensory axonal loss that could explain the absence of pain perception (Fig. 1f–h). Brain magnetic resonance imaging (MRI) was normal, and intellectual disability was not present. In both cases, a prominent hyperhidrosis was reported together with gastrointestinal dysfunction that necessitated temporary parenteral nutrition. Laparotomy in index subject 1 after alternating episodes of diarrhea and constipation showed a morphologically inconspicuous small intestine with reduced peristaltic waves and a grossly enlarged colon. Results from intestinal biopsies of both affected individuals were normal.

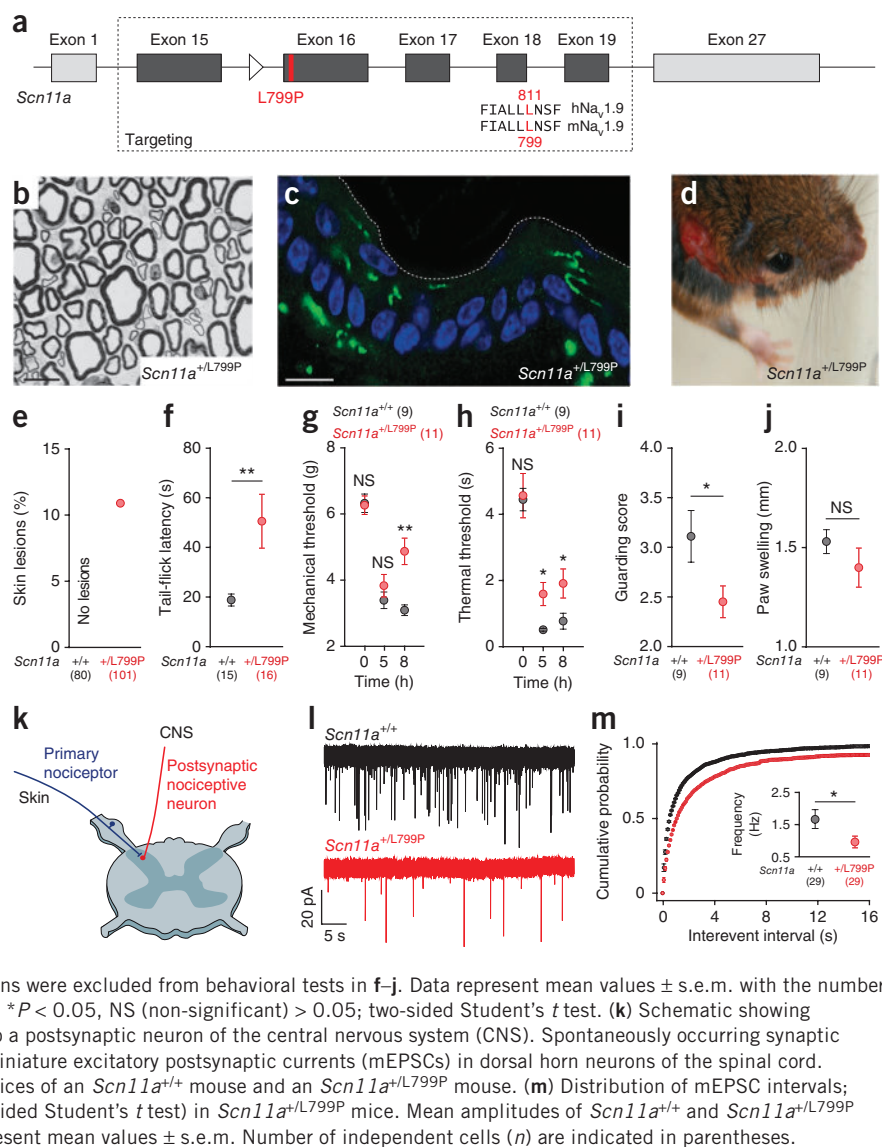
Our results imply that the p.Leu811Pro alteration in Na_v1.9 is disease causing. This finding may seem unexpected because the loss of Na_v1.9 in mice results in subtle sensory deficits, but it supports a role for this channel in the hyperexcitability of sensory neurons during inflammatory pain^{16–21}. To further address the pathogenicity of the human p.Leu811Pro alteration, we introduced the orthologous alteration (Na_v1.9 Leu799Pro) into the mouse *Scn11a* locus by homologous recombination (Fig. 2a and Supplementary Fig. 1).

Heterozygous knock-in mice (*Scn11a*^{+/^{L799P}) were viable and were born at the expected mendelian ratio.}

We verified expression of the mutant *Scn11a* allele in knock-in mice using mRNA from dorsal root ganglia (DRG) that harbor the cell bodies of nociceptors (Supplementary Fig. 2). We confirmed the presence of the missense mutation within the correctly spliced exons of the *Scn11a* transcript (Supplementary Fig. 2). No obvious morphological changes were detected in sensory axons or small nerve fibers in the skin of knock-in mice at 5 months of age (Fig. 2b,c and Supplementary Fig. 3). However, 11% of knock-in mice (*Scn11a*^{+/^{L799P}; *n* = 101) showed severe tissue lesions that were not observed in wild-type mice (*Scn11a*^{+/⁺; *n* = 80) (Fig. 2d,e). These lesions appeared to be self-inflicted because they also occurred in solitarily housed animals. *Scn11a*^{+/^{L799P} mice also exhibited a significantly higher threshold for noxious heat stimuli than wild-type littermates as determined by tail-flick experiments (Fig. 2f). Although the withdrawal threshold for plantar mechanical and thermal stimulation did not differ between genotypes under basal conditions, *Scn11a*^{+/^{L799P} mice showed a smaller reduction in the withdrawal threshold after zymosan-induced inflammation, indicating less thermal and mechanical hyperalgesia (Fig. 2g,h). *Scn11a*^{+/^{L799P} mice also showed less protective behavior (guarding) after zymosan application, a finding that is also in line with reduced pain sensitivity (Fig. 2i). Of note, swelling of the injected paw, which could influence guarding, was not different between the genotypes (Fig. 2j).}}}}}

The reduced pain sensitivity without obvious signs of neurodegeneration suggests a transmission defect from primary nociceptors to postsynaptic neurons (Fig. 2k). In agreement with the idea of reduced synaptic transmission from DRG neurons to spinal cord nociceptive neurons, miniature excitatory postsynaptic currents (mEPSCs) in acute spinal cord slices from *Scn11a*^{+/^{L799P} mice were less frequent compared to wild-type mice (*P* < 0.05; Fig. 2l,m).}

Figure 2 *Scn11a*^{+L799P} mice recapitulate aspects of the human phenotype. (a) Targeting construct with the nucleotide change c.2396T>C (p.Leu799Pro; red bar) in exon 16 of the *Scn11a* locus corresponding to p.Leu811Pro in human Na_v1.9. A neomycin cassette with flanking *loxP* sites for selection (remaining *loxP* site indicated as a triangle) was removed from intron 15 by Cre expression. The alignment of human Na_v1.9 (hNa_v1.9) and mouse (mNa_v1.9) protein sequences in the vicinity of the leucine residue of interest (red) is shown. (b) Semithin section of the sensory nerve distal to the fourth lumbar spinal nerve (L4) in *Scn11a*^{+L799P} mice did not show obvious morphological alterations. Scale bar, 10 μm. (c) Staining (green) for α-protein gene product 9.5 (PGP9.5) in the skin of *Scn11a*^{+L799P} mice showing regular innervation of the epidermis by small nerve fibers. Blue, DAPI; the dotted line marks the Stratum corneum. Scale bar, 15 μm. (d) Example of a tissue lesion in *Scn11a*^{+L799P} mice. (e) Tissue lesions were observed in 11% of *Scn11a*^{+L799P} mice. (f) Heat pain sensitivity (47 °C) was assessed by tail-flick tests on wild-type (*Scn11a*^{+/+}) and heterozygous (*Scn11a*^{+L799P}) mice at 3 months of age. (g,h) Plantar withdrawal thresholds to mechanical (g) and thermal (h) stimulation did not differ between genotypes (baseline, 0 h). Thermal and mechanical thresholds measured 5 and 8 h after intraplantar zymosan injection were higher in *Scn11a*^{+L799P} mice. (i) Less guarding in *Scn11a*^{+L799P} mice after local inflammation by intraplantar zymosan application as determined by gait-scoring test. (j) Paw swelling after zymosan injection to induce inflammation did not show significant differences between genotypes. Mice with skin lesions were excluded from behavioral tests in f–j. Data represent mean values ± s.e.m. with the numbers of mice indicated in parentheses in f–j. ***P* < 0.01, **P* < 0.05, NS (non-significant) > 0.05; two-sided Student's *t* test. (k) Schematic showing the connection of a peripheral nociceptive neuron to a postsynaptic neuron of the central nervous system (CNS). Spontaneously occurring synaptic events caused by vesicle release are measured by miniature excitatory postsynaptic currents (mEPSCs) in dorsal horn neurons of the spinal cord. (l) Representative mEPSC traces from spinal cord slices of an *Scn11a*^{+/+} mouse and an *Scn11a*^{+L799P} mouse. (m) Distribution of mEPSC intervals; inset, mEPSCs were less frequent (**P* < 0.05; two-sided Student's *t* test) in *Scn11a*^{+L799P} mice. Mean amplitudes of *Scn11a*^{+/+} and *Scn11a*^{+L799P} mice were not different (data not shown). Data represent mean values ± s.e.m. Number of independent cells (*n*) are indicated in parentheses. Cells were obtained from five mice per genotype.

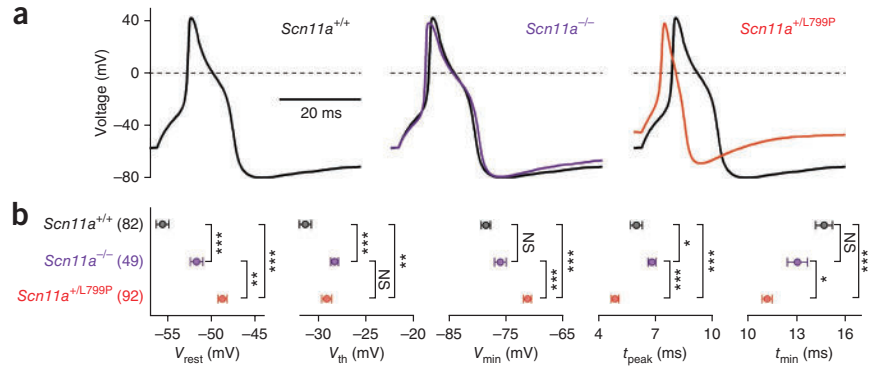


Owing to its unique electrophysiological properties, Na_v1.9 has been suggested to positively influence the excitability of DRG neurons²². We therefore investigated the electrical properties of DRG neurons isolated from mice. The resting membrane potential (V_{rest}) of DRG neurons from *Scn11a*^{+L799P} mice was shifted by 6.7 mV compared to wild-type mice ($P < 0.001$), indicating that a significant fraction of the mutant Na_v1.9 channels are active under resting conditions (Fig. 3a,b). In *Scn11a*^{+L799P} cells, the duration of action potentials was also significantly reduced ($P < 0.001$), and the hyperpolarization occurring afterwards was less pronounced ($P < 0.001$). In contrast, the absence of functional Na_v1.9 channels in DRG neurons from knockout mice (*Scn11a*^{-/-}) increased V_{rest} by 3.7 mV ($P < 0.001$) and the firing threshold for action potentials by 2 mV ($P < 0.001$) but had no major impact on other action-potential characteristics (Fig. 3a,b). The mouse Na_v1.9 Leu799Pro missense alteration thus results in a prominent phenotype in DRG neurons, whereas loss of the channel has only a minor effect on action potentials.

Current recordings under voltage-clamp control of neurons from wild-type mice (*Scn11a*^{+/+}), neurons solely harboring mutant channels (*Scn11a*^{-L799P}) and neurons from *Scn11a*^{+L799P} mice showed

that the missense alteration permits functional channels (Fig. 4a and Supplementary Fig. 4). Compared to wild-type cells, *Scn11a*^{+L799P} and *Scn11a*^{-L799P} cells had diminished peak current densities at depolarized voltages (Fig. 4b). In *Scn11a*^{+L799P} neurons in particular, a greater inward current was observed under resting conditions (Fig. 4b, inset). This augmentation of channel activity at rest was caused by a leftward shift in the voltage dependence of activation by -26 mV, as estimated with equation (1) (Online Methods). The alteration furthermore strongly slowed down the kinetics of channel deactivation (Fig. 4c). The effect was compatible with a mutation-induced shift in the voltage dependence of the deactivation kinetics by -45 mV that did not affect the associated apparent gating charge transfer (Fig. 4d). The mixed channel population in *Scn11a*^{+L799P} neurons displayed a fast and a slow deactivating component with a relative fraction of mutant channels of 0.38 ± 0.03 (Fig. 4d). Channel inactivation was more pronounced in *Scn11a*^{-L799P} cells than in wild-type cells (Fig. 4e). Voltage dependence was shifted by -29 mV, effectively reducing the availability of the mutant (Fig. 4f). Channels in *Scn11a*^{+L799P} cells inactivated with two components, one resembling the behavior of wild-type channels and the other resembling

Figure 3 Electrophysiological properties of mouse DRG neurons. **(a)** Action potentials, elicited by the injection of 100–200 pA for 10 ms, were recorded from isolated small-diameter DRG neurons in the current-clamp mode. For reference, wild-type traces (*Scn11a*^{+/+}) are also shown with traces for *Scn11a* knockout (*Scn11a*^{-/-}) and heterozygous Leu799Pro knock-in cells (*Scn11a*^{+L799P}). Only DRG neurons with a diameter less than 24 μ m were analyzed; their mean electrical cell membrane capacitances, as a measure of cell size, were 12.1 ± 0.3 pF (*Scn11a*^{+/+}; $n = 82$), 11.3 ± 0.4 pF (*Scn11a*^{-/-}; $n = 49$) and 12.9 ± 0.3 pF (*Scn11a*^{+L799P}; $n = 92$). **(b)** Parameters characterizing action potentials include resting membrane potential (V_{rest}), action potential threshold (V_{th}), maximal after-hyperpolarization (V_{min}), time to peak (t_{peak}) and time from peak to minimum (t_{min}). Data represent mean values \pm s.e.m. with numbers of experiments from at least three mice given in parentheses. Significance was tested with a two-sided Student's t test. *** $P < 0.001$, ** $P < 0.01$, * $P < 0.05$, NS > 0.05 .

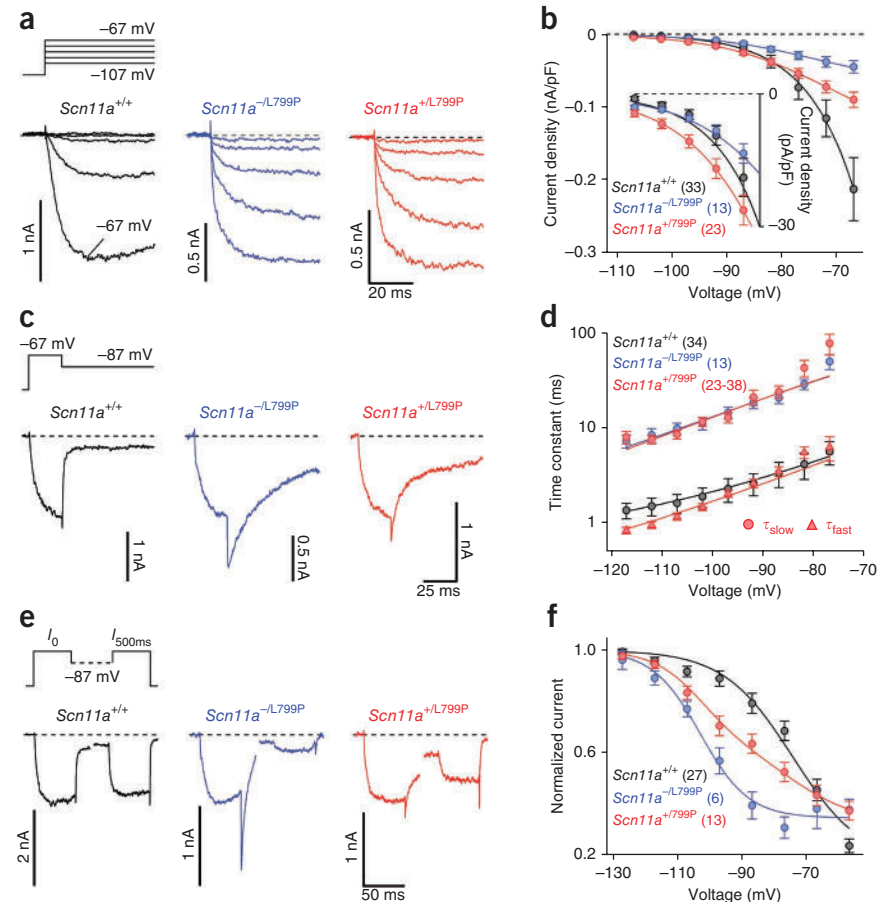


the behavior of mutant channels (**Fig. 4f**). The fraction of mutant channels was estimated to be 0.35 ± 0.02 .

The results indicate that mouse $Na_v1.9$ Leu799Pro channels mediate sodium ion currents that are activated, even if the cell membrane

is hyperpolarized. However, a quantitative assessment is compromised by the overlapping expression of $Na_v1.8$ channels in DRG neurons. To circumvent this limitation and to analyze the human mutation, we heterologously expressed human $Na_v1.9$ and $Na_v1.9$ Leu811Pro

Figure 4 Mutant $Na_v1.9$ channels display gain-of-function properties. **(a)** Current recordings from DRG neurons of wild-type (*Scn11a*^{+/+}), monoallelic Leu799Pro knock-in (*Scn11a*^{-L799P}) and heterozygous knock-in (*Scn11a*^{+L799P}) mice. **(b)** Mean current density as a function of voltage was fitted to estimate the voltage dependence of channel opening and yielded half-maximal activation at -45.2 ± 8.0 mV (*Scn11a*^{+/+}) and -70.8 ± 2.2 mV (*Scn11a*^{-L799P}); slope factors were 7.7 ± 0.2 mV and 9.4 ± 0.5 mV, respectively. The voltage dependence of channel opening for neurons from *Scn11a*^{+L799P} mice was described by a linear combination of both components with equal weight. Inset, 10 \times magnification of the voltage range between -107 and -87 mV illustrating the increased current density of neurons from *Scn11a*^{+L799P} mice under resting conditions ($P < 0.05$ between -107 and -87 mV). **(c)** Current recordings at -87 mV demonstrating rapid (*Scn11a*^{+/+}) and slow (*Scn11a*^{-L799P}) deactivation kinetics. Biphasic deactivation with a fast and a slow component for channels from *Scn11a*^{+L799P} mice resembled the deactivation of wild-type and mutant channels. **(d)** Single-exponential tail current time constants as a function of voltage. Voltage dependence for channels from *Scn11a*^{-L799P} mice was shifted by about -45 mV with respect to wild-type channels; the symmetry factor of the activation barrier (δ) was set to 0.5, and the charge transfer was $4.8 \pm 1.8 e_0$. Double-exponential deactivation time constants of tail currents recorded from channels from *Scn11a*^{+L799P} mice are superimposed. The voltage dependence of the slow component (τ_{slow}) was shifted by -45 mV with respect to the fast component (τ_{fast}), assuming a charge transfer identical to that of channels from *Scn11a*^{+/+} and *Scn11a*^{-L799P} mice. **(e)** Whole-cell current traces obtained from DRG neurons of the indicated genotype before (I_0) and after (I_{500ms}) 500-ms conditioning at -87 mV demonstrating steady-state inactivation. **(f)** Steady-state inactivation of currents of channels from *Scn11a*^{+/+} and *Scn11a*^{-L799P} mice was analyzed with Boltzmann functions, yielding half-maximal inactivation at -74.4 ± 2.2 mV (*Scn11a*^{+/+}) and -102.9 ± 1.4 mV (*Scn11a*^{-L799P}), with slope factors of 10.7 ± 2.2 mV and 7.4 ± 1.2 mV, respectively. Inactivation of channels from *Scn11a*^{+L799P} mice displayed two components, described with a linear combination of components with parameters from wild-type and mutant channels ($35 \pm 2\%$ mutant channels). All data represent mean values \pm s.e.m. with numbers of experiments given in parentheses.



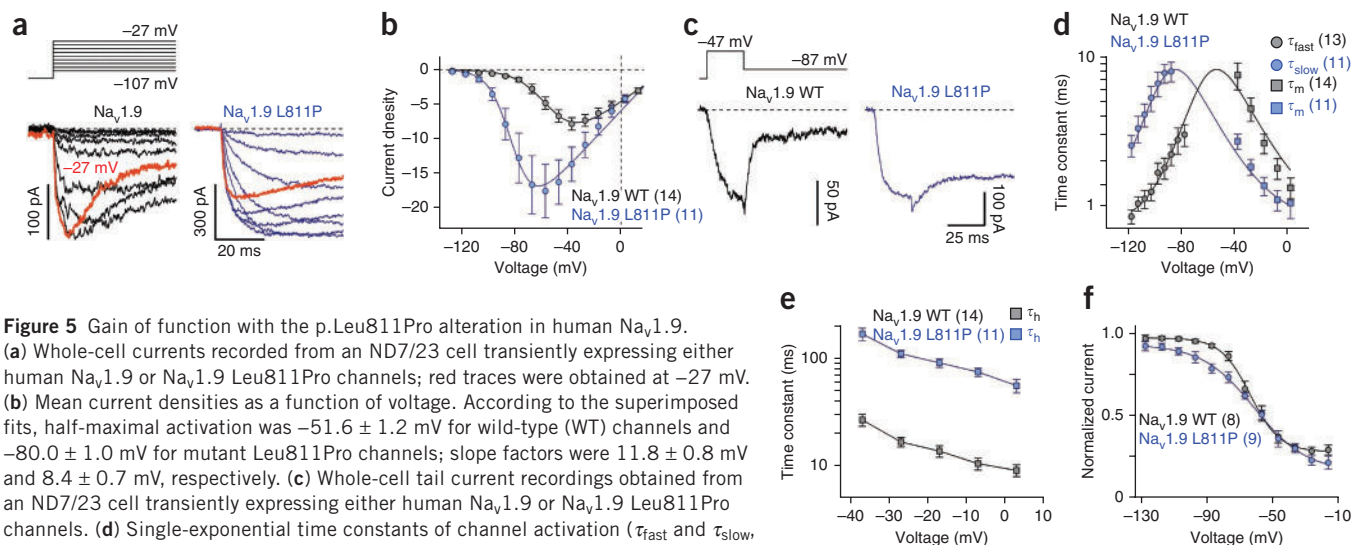


Figure 5 Gain of function with the p.Leu811Pro alteration in human $\text{Na}_v1.9$.

(a) Whole-cell currents recorded from an ND7/23 cell transiently expressing either human $\text{Na}_v1.9$ or $\text{Na}_v1.9$ Leu811Pro channels; red traces were obtained at -27 mV. (b) Mean current densities as a function of voltage. According to the superimposed fits, half-maximal activation was -51.6 ± 1.2 mV for wild-type (WT) channels and -80.0 ± 1.0 mV for mutant Leu811Pro channels; slope factors were 11.8 ± 0.8 mV and 8.4 ± 0.7 mV, respectively. (c) Whole-cell tail current recordings obtained from an ND7/23 cell transiently expressing either human $\text{Na}_v1.9$ or $\text{Na}_v1.9$ Leu811Pro channels. (d) Single-exponential time constants of channel activation (τ_{fast} , squares) and deactivation (τ_m , circles) as a function of voltage. The continuous curves are data fits according to equation (5) (Online Methods), yielding a charge transfer of $6.0 \pm 1.8 e_0$ and a symmetry factor of 0.6 ± 0.2 ; the voltage dependence of the Leu811Pro mutant was shifted by -31.0 ± 7.8 mV. (e) Single-exponential time constants of inactivation as a function of voltage. Straight lines connect the data points for clarity. (f) Steady-state inactivation, described with Boltzmann fits (equation (3); Online Methods), yielding half-maximal inactivation at -63.9 ± 0.6 mV and -61.4 ± 1.4 mV for wild-type and mutant Leu811Pro channels, respectively; the corresponding slope factors were 8.9 ± 0.5 mV and 15.7 ± 1.4 mV. All data represent mean values \pm s.e.m. with numbers of experiments given in parentheses.

mutant channels in ND7/23 cells²³ (Fig. 5a). Mutant Leu811Pro channels showed a shift in the voltage dependence of activation by -28 mV, significantly increased current density at resting voltages ($P < 0.01$ between -107 and -47 mV; Fig. 5b) and decelerated channel deactivation (Fig. 5c). Using a simple one-step gating scheme as an operational data descriptor (equation (5); Online Methods), we found that the p.Leu811Pro alteration caused a shift in the voltage dependencies of activation and deactivation kinetics by about -30 mV (Fig. 5d). In addition, the single-exponential kinetics of channel inactivation between -37 and 3 mV were slowed down by sixfold (Fig. 5e). The half-maximal voltage of steady-state inactivation was not markedly altered, but the slope factor was reduced by a factor of two (Fig. 5f). Thus, the phenotype of human $\text{Na}_v1.9$ Leu811Pro channels largely resembles that of mouse $\text{Na}_v1.9$ Leu799Pro channels, except in terms of steady-state inactivation. The weak influence of the alteration on inactivation in the human channel is compatible with a stronger gain-of-function effect and, likely, with a more pronounced phenotype than that observed in knock-in mice.

Our data demonstrate that the p.Leu811Pro alteration results in a prominent gain-of-function phenotype mediated by a leftward shift in channel activation and deactivation kinetics as well as by a slow-down in channel inactivation. The altered residue, located at the distal end of the S6 segment in domain II (Fig. 1b), thus interferes with the process of voltage-dependent gate closure and channel inactivation. Both aspects are compatible with the contemporary knowledge on Na_v channel function, in which S6 segments constitute part of the channel gate, with their C-terminal ends forming acceptors for the inactivation domain (IFM motif; Fig. 1b)^{24,25}. The p.Leu811Pro alteration increases the basal activity of $\text{Na}_v1.9$ channels, resulting in excess sodium ion influx at rest and subsequent cell depolarization. Consequently, other ion channels such as $\text{Na}_v1.7$, $\text{Na}_v1.8$ and voltage-gated calcium ion channels that form the main constituents of the action potential in DRG neurons may undergo progressive inactivation, resulting in a conduction block. This hypothesis is also supported by the observation that the prominent shoulder of DRG neuron action potentials necessary for mediating calcium ion influx is

blunted in $\text{Scn11a}^{+/L799P}$ neurons (Fig. 3a,b). Insufficient activation of calcium ion channels consequently results in impaired neurotransmitter release at presynaptic nerve terminals to transmit pain signals to the spinal cord^{26,27}. This mechanism might also cause chronic desensitization of pain-processing pathways.

The finding of a gain-of-function mechanism in this channelopathy strongly contrasts with previously described pain-related sodium channel disorders. Whereas an inability to experience pain is caused by loss-of-function alterations in the homologous $\text{Na}_v1.7$ channel encoded by SCN9A ⁹, heterozygous gain-of-function mutations in SCN9A lead to devastating pain attacks^{28–30}. Gain of function in SCN9A and SCN10A can also result in small-fiber neuropathy, characterized by neuropathic pain due to degeneration of the terminals of thinly myelinated A δ and unmyelinated C fibers^{29,31,32}. In contrast, gain of SCN11A function does not increase pain sensation but rather blocks the transmission of pain signals.

Muscular weakness in the affected individuals might be attributed to a developmental role of the channel in motor neurons, as $\text{Na}_v1.9$ was shown to contribute to the spontaneous neural activity that promotes axon growth in these neurons^{33,34}. Prominent hyperhidrosis and gastrointestinal malfunction in the affected individuals may be a consequence of autonomic dysfunction. $\text{Na}_v1.9$ is indeed expressed in pacemaker neurons of the intestinal tract of rodents, and Scn11a knockout mice display altered colonic motility^{35–37}.

In summary, an SCN11A channelopathy should be considered in individuals with a congenital insensitivity to pain, muscular hypotonia and gastrointestinal disturbances. Because the individuals reported here showed no obvious signs of neurodegeneration, specific sodium channel antagonists might be a potential treatment option. Modulation of $\text{Na}_v1.9$ might also be a conceivable treatment option in common disorders such as chronic pain or gastrointestinal motility disturbances.

URLs. 1000 Genomes Project, <http://www.1000genomes.org/>; Variant Effect Predictor, <http://www.ensembl.org/tools.html>; Exome Variant Server, National Heart, Lung, and Blood Institute (NHLBI) Exome

Sequencing Project (ESP), <http://evs.gs.washington.edu/EVS/>; Online Mendelian Inheritance in Man (OMIM), <http://www.omim.org/>; Varbank, <https://anubis.ccg.uni-koeln.de/varbank/>; DeNovoGear, <http://sourceforge.net/projects/denovogear/>.

METHODS

Methods and any associated references are available in the [online version of the paper](#).

Accession codes. Human *SCN11A*, [NM_014139.2](#); mouse *Scn11a*, [NM_011887.3](#).

Note: Any Supplementary Information and Source Data files are available in the online version of the paper.

ACKNOWLEDGMENTS

We are grateful to the families participating in the study. Excellent technical assistance was provided by K. Schorr, A. Roßner, P. Schroth and the team from the Jena University Hospital animal facility. *Scn11a*^{-/-} mice were generously provided by J.N. Wood (Wolfson Institute for Biomedical Research, University College London). ND7/23 cells were generously provided by C. Nau (University Hospital Erlangen). We thank D.G.G. McMillan for critical reading of the manuscript. This work was supported by grants from the DFG (Deutsche Forschungsgemeinschaft) to I.K. (KU 1587/2-1) and C.A.H. (HU 800/5-1, RTG 1715, HU 800/6-1 and HU 800/7-1). Funding to J.B., P.D.J. and V.T. was provided by the University of Antwerp, Fund for Scientific Research (FWO-Flanders), Association Belge contre les Maladies neuro-Musculaires (ABMM) and Medical Foundation Queen Elisabeth (GSKE). Funding to R.B. was provided by the DFG (BL567/3-1). Funding to J.W. was provided by the DFG (WE 1406/13-1) and IZKF (Interdisziplinäres Zentrum für Klinische Forschung) Aachen (N5-3).

AUTHOR CONTRIBUTIONS

I.K., C.A.H., E.L. and S.H.H. designed this study. G.C.K., J.B., V.T., P.D.J. and T.S. assessed the phenotypes of the affected individuals. M.B. and J.W. performed neuropathological analysis. J.A., H.T. and P.N. performed exome sequencing. Additional experiments were performed by I.K. (genetics, generation of knock-in mice and molecular biology), E.L., R.O.G. and L.L. (electrophysiology), S.G. (molecular biology and histology), J.C.H., A.W. and R.B. (molecular biology) and T.H. (tail-flick assay and histology). M.E. and H.-G.S. performed behavioral analysis and evaluation. I.K., L.L., E.L., S.H.H. and C.A.H. analyzed the data and wrote the manuscript with input from the coauthors.

COMPETING FINANCIAL INTERESTS

The authors declare no competing financial interests.

Reprints and permissions information is available online at <http://www.nature.com/reprints/index.html>.

- Basbaum, A.I., Bautista, D.M., Scherrer, G. & Julius, D. Cellular and molecular mechanisms of pain. *Cell* **139**, 267–284 (2009).
- Williams, F.M. *et al.* Genes contributing to pain sensitivity in the normal population: an exome sequencing study. *PLoS Genet.* **8**, e1003095 (2012).
- Woolf, C.J. & Salter, M.W. Neuronal plasticity: increasing the gain in pain. *Science* **288**, 1765–1769 (2000).
- Dib-Hajj, S.D., Cummins, T.R., Black, J.A. & Waxman, S.G. Sodium channels in normal and pathological pain. *Annu. Rev. Neurosci.* **33**, 325–347 (2010).
- Eijkelkamp, N. *et al.* Neurological perspectives on voltage-gated sodium channels. *Brain* **135**, 2585–2612 (2012).
- Gold, M.S. & Gebhart, G.F. Nociceptor sensitization in pain pathogenesis. *Nat. Med.* **16**, 1248–1257 (2010).
- Kurth, I. *et al.* Mutations in *FAM134B*, encoding a newly identified Golgi protein, cause severe sensory and autonomic neuropathy. *Nat. Genet.* **41**, 1179–1181 (2009).
- Rotthier, A., Baets, J., Timmerman, V. & Janssens, K. Mechanisms of disease in hereditary sensory and autonomic neuropathies. *Nat. Rev. Neurol.* **8**, 73–85 (2012).
- Cox, J.J. *et al.* An *SCN9A* channelopathy causes congenital inability to experience pain. *Nature* **444**, 894–898 (2006).
- Yuan, J. *et al.* Hereditary sensory and autonomic neuropathy type IID caused by an *SCN9A* mutation. *Neurology* **80**, 1641–1649 (2013).
- Li, H. & Durbin, R. Fast and accurate long-read alignment with Burrows-Wheeler transform. *Bioinformatics* **26**, 589–595 (2010).
- Conrad, D.F. *et al.* Variation in genome-wide mutation rates within and between human families. *Nat. Genet.* **43**, 712–714 (2011).
- Abecasis, G.R. *et al.* A map of human genome variation from population-scale sequencing. *Nature* **467**, 1061–1073 (2010).
- Veltman, J.A. & Brunner, H.G. *De novo* mutations in human genetic disease. *Nat. Rev. Genet.* **13**, 565–575 (2012).
- Cummins, T.R. *et al.* A novel persistent tetrodotoxin-resistant sodium current in SNS-null and wild-type small primary sensory neurons. *J. Neurosci.* **19**, RC43 (1999).
- Amaya, F. *et al.* The voltage-gated sodium channel Na_v1.9 is an effector of peripheral inflammatory pain hypersensitivity. *J. Neurosci.* **26**, 12852–12860 (2006).
- Leo, S., D’Hooge, R. & Meert, T. Exploring the role of nociceptor-specific sodium channels in pain transmission using Na_v1.8 and Na_v1.9 knockout mice. *Behav. Brain Res.* **208**, 149–157 (2010).
- Lolignier, S. *et al.* Na_v1.9 channel contributes to mechanical and heat pain hypersensitivity induced by subacute and chronic inflammation. *PLoS ONE* **6**, e23083 (2011).
- Maingret, F. *et al.* Inflammatory mediators increase Na_v1.9 current and excitability in nociceptors through a coincident detection mechanism. *J. Gen. Physiol.* **131**, 211–225 (2008).
- Östman, J.A., Nassar, M.A., Wood, J.N. & Baker, M.D. GTP up-regulated persistent Na⁺ current and enhanced nociceptor excitability require Na_v1.9. *J. Physiol. (Lond.)* **586**, 1077–1087 (2008).
- Priest, B.T. *et al.* Contribution of the tetrodotoxin-resistant voltage-gated sodium channel Na_v1.9 to sensory transmission and nociceptive behavior. *Proc. Natl. Acad. Sci. USA* **102**, 9382–9387 (2005).
- Herzog, R.I., Cummins, T.R. & Waxman, S.G. Persistent TTX-resistant Na⁺ current affects resting potential and response to depolarization in simulated spinal sensory neurons. *J. Neurophysiol.* **86**, 1351–1364 (2001).
- Vanoye, C.G., Kunic, J.D., Ehring, G.R. & George, A.L. Jr. Mechanism of sodium channel Na_v1.9 potentiation by G-protein signaling. *J. Gen. Physiol.* **141**, 193–202 (2013).
- Catterall, W.A. From ionic currents to molecular mechanisms: the structure and function of voltage-gated sodium channels. *Neuron* **26**, 13–25 (2000).
- Payandeh, J., Scheuer, T., Zheng, N. & Catterall, W.A. The crystal structure of a voltage-gated sodium channel. *Nature* **475**, 353–358 (2011).
- Huang, Z. *et al.* Presynaptic HCN1 channels regulate Ca_v3.2 activity and neurotransmission at select cortical synapses. *Nat. Neurosci.* **14**, 478–486 (2011).
- Jacus, M.O., Uebele, V.N., Renger, J.J. & Todorovic, S.M. Presynaptic Ca_v3.2 channels regulate excitatory neurotransmission in nociceptive dorsal horn neurons. *J. Neurosci.* **32**, 9374–9382 (2012).
- Cheng, X. *et al.* Deletion mutation of sodium channel Na_v1.7 in inherited erythromelalgia: enhanced slow inactivation modulates dorsal root ganglion neuron hyperexcitability. *Brain* **134**, 1972–1986 (2011).
- Dib-Hajj, S.D., Yang, Y., Black, J.A. & Waxman, S.G. The Na_v1.7 sodium channel: from molecule to man. *Nat. Rev. Neurosci.* **14**, 49–62 (2013).
- Fertleman, C.R. *et al.* *SCN9A* mutations in paroxysmal extreme pain disorder: allelic variants underlie distinct channel defects and phenotypes. *Neuron* **52**, 767–774 (2006).
- Faber, C.G. *et al.* Gain of function Na_v1.7 mutations in idiopathic small fiber neuropathy. *Ann. Neurol.* **71**, 26–39 (2012).
- Faber, C.G. *et al.* Gain-of-function Na_v1.8 mutations in painful neuropathy. *Proc. Natl. Acad. Sci. USA* **109**, 19444–19449 (2012).
- Subramanian, N. *et al.* Role of Na_v1.9 in activity-dependent axon growth in motoneurons. *Hum. Mol. Genet.* **21**, 3655–3667 (2012).
- Wetzel, A., Jablonka, S. & Blum, R. Cell-autonomous axon growth of young motoneurons is triggered by a voltage-gated sodium channel. *Channels (Austin)* **7**, 51–56 (2013).
- Copel, C., Clerc, N., Osorio, N., Delmas, P. & Mazet, B. The Na_v1.9 channel regulates colonic motility in mice. *Front. Neurosci.* **7**, 58 (2013).
- Rugiero, F. *et al.* Selective expression of a persistent tetrodotoxin-resistant Na⁺ current and Na_v1.9 subunit in myenteric sensory neurons. *J. Neurosci.* **23**, 2715–2725 (2003).
- Copel, C. *et al.* Activation of neurokinin 3 receptor increases Na_v1.9 current in enteric neurons. *J. Physiol. (Lond.)* **587**, 1461–1479 (2009).

ONLINE METHODS

Subjects. This study was approved by the local research ethics committees of the participating institutions. Consent was given for publication of the photographs.

Whole-exome sequencing. For whole-exome sequencing, 1 µg of DNA was fragmented using sonification technology (Covaris). Fragments were end repaired and adaptor ligated, including incorporation of sample index barcodes. After size selection, libraries were subjected to the enrichment process (Agilent SureSelect XT2 Human All Exon v4, Agilent Technologies). Samples were pooled and sequenced on one lane of an Illumina HiSeq 2000 sequencing instrument using a paired-end 2 × 100-bp protocol.

For the trio (father/mother/child), this sequencing resulted in 13.3/13.8/11.6 Gb of mapped sequences, respectively, with mean coverages of 118/123/104× and 30× coverages of 82/90/86% of target sequences. For data analysis, the Varbank pipeline v.2.3 and interface was used (H.T., S. Motameny, A. Kawalia, K. Jabbar, W. Gunia *et al.*, unpublished data; see URLs). Primary data were filtered according to signal purity by Illumina Real-Time Analysis (RTA) software v1.8. Subsequently, reads were mapped to the human genome reference build hg19 using the BWA alignment algorithm. Genome Analysis Toolkit (GATK) v1.6 was used to mark duplicated reads, perform local realignment around short indels, recalibrate base quality scores and call SNPs and short indels.

Calling of *de novo* SNVs and short indels was performed using FIGL¹², which has been implemented into the software DeNovoGear (version 0.5.2; see URLs). First, SAMtools mpileup (version 0.1.7) was used to report genotype likelihoods, and we then calculated the posterior probability of the variant being a *de novo* mutation (pp_dnm) versus being consistent with mendelian inheritance (pp_null). Calls were then filtered for pp_null < pp_dnm > 0.8.

Sanger sequencing of *SCN11A* exons was performed using standard procedures. Primer sequences are available upon request.

Nerve pathology. Nerves were fixed in 3.9% glutaraldehyde, embedded in epoxy resin and further processed for semithin-section light microscopy and ultrathin-section electron microscopy as described previously³⁸.

Generation of targeted *Scn11a*^{+L799P} knock-in mice. A 14.5-kb KpnI-XbaI fragment of the BAC clone RP23-346E22 containing exons 15–19 of the mouse *Scn11a* gene was subcloned into the pKS vector. A *pgk* promoter-driven neomycin resistance cassette (*neo*) flanked by *loxP* sites was inserted into the AatII site in intron 15. The nucleotide at position chr. 9: 119,784,155 (mouse assembly GRCm38/mm10) (c.2396T; NM_011887.3, numbering beginning from the start codon ATG at position 53–55) in exon 16 was replaced by cytosine via PCR-based mutagenesis and replaced an MluI-KasI fragment. This resulted in the sequence encoding the missense alteration p.Leu799Pro in the murine Na_v1.9 protein (NP_036017.3). Mice are designated as wild-type (*Scn11a*^{+/+}), heterozygous (*Scn11a*^{+L799P}) or homozygous (*Scn11a*^{L799P/L799P}) knock-in mice. All coding exons and adjacent splice sites of the targeting vector were verified via sequencing. Homologous recombination to the *Scn11a* locus was verified by long-range PCR (Supplementary Fig. 1). The primer combination LR1–LR2 resulted in a 3,742-bp amplicon in case of homologous recombination. LR1 is located 5′ to the targeting vector; LR2 is located in the *neo* cassette. Primers LR3 (located in intron 15) and LR4 (located 3′ to the targeting vector) resulted in a 6,086-bp product. The purified LR3–LR4 amplicon was sequenced with regard to the presence of the missense mutation in LR1–LR2-positive embryonic stem cell clones. Embryonic stem cell clones were injected into C57BL/6 blastocysts to generate chimeras. Resulting mice were crossed with Cre deleter mice to remove the *neo* cassette and were backcrossed with C57BL/6 mice³⁹. Studies were performed in a mixed 129SV/C57BL/6 background in the F₂ and F₃ generations. *Scn11a* knockout mice (*Scn11a*^{-/-}) used in this study have been reported previously²⁰. ‘Monoallelic’ *Scn11a*^{-L799P} mice were generated by crossing *Scn11a*^{-/-} mice with *Scn11a*^{+L799P} mice. Animal care and experimental procedures were performed in accordance with the guidelines established by the animal welfare committee of the University of Jena.

Mouse genotyping. Genotyping of *Scn11a*^{+L799P} knock-in mice was performed with primers adjacent to the *loxP* site (geno-for, within the *Scn11a*

locus; geno-rev, sequence adjacent to the *loxP* site). For primer sequences, see Supplementary Table 1. PCR results in a 272-bp amplicon for the knock-in allele. PCR-positive mice were further genotyped by direct sequencing of the missense mutation in genomic DNA. Genotyping of *Scn11a*^{-/-} mice was reported previously²⁰.

Pain-related behavioral assays. *Mechanical and thermal withdrawal thresholds at the paw.* Behavioral tests were performed as previously described⁴⁰. Briefly, mechanical and thermal hyperalgesia at the hindpaws were assessed on adult male and female *Scn11a*^{+/+} and *Scn11a*^{+L799P} littermates before and after injection of zymosan (Sigma-Aldrich) into one hindpaw (injection volume of 20 µl at a concentration of 12.5 mg/ml in 0.1 M PBS, pH 7.4). Mice were placed into testing devices and, after their accommodation to the environment, mechanical withdrawal thresholds were determined with a dynamic plantar aesthesiometer (Ugo Basile), which applied increasing pressure (stimulus increase rate of 1 g/s; cutoff value of 10 g) to the paw. The weight force needed to elicit leg withdrawal reflecting the respective mechanical threshold was averaged from up to three consecutive stimuli. Two recordings before zymosan injection defined the baseline. Thermal hyperalgesia was assessed using the Hargreaves plantar test (Ugo Basile). Two consecutive standardized heat stimuli were applied to the paw for evaluation of mean latency (cutoff value of 20 s). Swelling was assessed by measuring the dorsoventral diameter of both hindpaws using an Oditest vernier caliper (Kroepelin).

Guarding scores. Gait abnormalities of the ipsilateral hindlimb were scored as previously described⁴¹: 0, normal walking; 1, slight limping; 2, persistent severe limping (still touching the floor); 3, severe limping with partial guarding of ipsilateral hindlimb (sometimes not touching the floor); 4, mainly guarding ipsilateral hindlimb (most times not touching the floor); 5, no walking at all.

Tail-flick assays. Thermal stimulation (at 47 °C) was applied to the tail of adult male *Scn11a*^{+/+} and *Scn11a*^{+L799P} littermates after their habituation to the test environment using the water immersion method. The time from onset of stimulation to rapid movement of the tail was recorded. Two separate determinations of tail-flick latency per mouse were recorded and averaged. Statistical comparisons of two groups of data were made using the two-sided Student’s *t* test.

The experimenter was blinded to the genotype of the mice in all behavioral tests.

Immunohistochemistry. Cryosections (15 µm) of 4% paraformaldehyde-fixed skin tissue from 5-month-old mice were stained with antibody to α-PGP9.5 (AbD serotec, 78630504; 1:1,000 dilution) using standard procedures. Images were acquired with a Leica TCS SP5 confocal scanning fluorescence microscope. For semithin sections, mice were perfused with 50 ml of fixative (4% paraformaldehyde, 1% glutaraldehyde). Sensory nerves were removed distal to the L4 DRG of the mouse, post-fixed overnight at 4 °C and cut approximately 5 mm distal to the dorsal root.

cDNA constructs for human Na_v1.9 and Na_v1.9 Leu811Pro. Human *SCN11A* (Na_v1.9) cDNA in pcDNA3.1 was described previously⁴². The clone was corrected for two variants that are not annotated in the current GenBank entry (NM_014139.2) using PCR-based mutagenesis. The p.Leu811Pro alteration was introduced by PCR-based mutagenesis and replaced a PshAI-XcmI fragment of the cDNA. The coding sequence of both constructs was verified by sequencing.

Quantitative RT-PCR. Quantitative PCR was performed using standard procedures. Briefly, total RNA was isolated from five DRGs, and cDNA was generated using SuperScript II (Invitrogen) with random hexamers (Invitrogen). Primer sequences for *Scn11a* and *Hprt* (used for normalization) are given in Supplementary Table 1.

Preparation of mouse DRG neurons. Mice were euthanized via cervical dislocation under anesthesia. DRG neurons were extracted from all levels of the spinal cord and were further processed according to a procedure adopted from Dib-Hajj *et al.*⁴³. Electrophysiological recordings were conducted within 24 h of extraction.

Electrophysiology. Patch pipettes were fabricated from Kimax borosilicate glass of about 1.0–2.5 M Ω resistance. An EPC-10 patch-clamp amplifier operated by PatchMaster software (HEKA Elektronik) was used. Series resistance was corrected electronically up to 85%. All recordings were performed at room temperature (20–22 °C), and all voltages were corrected for liquid junction potential. Current and voltage recordings were obtained in the whole-cell configuration of the patch-clamp method from isolated small DRG neurons with an electrical capacitance of less than 20 pF, to restrict the recordings mostly to C fiber neurons. Bath solutions for current-clamp recordings contained 120 mM NaCl, 3 mM KCl, 2.5 mM CaCl₂, 1 mM MgCl₂, 30 mM HEPES and 15 mM glucose (pH 7.4 with NaOH) and for the pipette contained 125 mM KCl, 8 mM NaCl, 1 mM CaCl₂, 1 mM MgCl₂, 0.4 mM Na₂-GTP, 4 mM Mg-ATP, 10 mM EGTA and 10 mM HEPES (pH 7.3 with KOH). For voltage-clamp recordings, the bath contained 150 mM NaCl, 2 mM KCl, 1.5 mM CaCl₂, 1 mM MgCl₂ and 10 mM HEPES (pH 7.4 with NaOH) and was supplemented with 0.1 mM CdCl₂ and 0.0005 mM tetrodotoxin for recordings from DRG neurons and with 0.0003 mM tetrodotoxin for recordings from ND7/23 cells; the intracellular pipette solution contained 35 mM NaCl, 105 mM CsF, 10 mM EGTA and 10 mM HEPES (pH 7.3 with CsOH). The application of tetrodotoxin blocked all Na_v channels with the exception of Na_v1.8 and Na_v1.9, and employing fluoride as an intracellular anion enabled us to measure Na_v1.9-mediated currents up to –67 mV without interference of the Na_v1.8 currents that are typically larger (Supplementary Fig. 4).

Current-clamp recordings. Resting membrane voltage was measured by zero-current injection directly after forming the whole-cell configuration. Subsequently, single action potentials were evoked by injecting a current of 100–200 pA for a period of 10 ms followed by a 200-ms pulse without current injection. The sampling interval for voltage measurements was 50 μ s. The firing threshold of an action potential was defined as the voltage at which dV/dt reached the level of $0.03 \times (dV/dt_{\max} - dV/dt_{\min}) + dV/dt_{\min}$.

Voltage-clamp recordings. To ensure recovery from inactivation during current measurements, the membrane holding potential was set to –127 mV in DRG neurons and to –147 mV in ND7/23 cells. Data were low-pass filtered at 5 kHz and digitized with a sampling interval of 40 μ s. Leak and capacitive currents were measured at –107 or –147 mV (DRG) and –127 or –167 mV (ND7/23 cells) and subtracted manually.

Human Na_v1.9 channels and mutant Na_v1.9 Leu811Pro channels were transiently expressed in ND7/23 cells as described recently²³. Transfected cells were identified by coexpression of CD8 and by incubating the cells with microbeads coated with antibody to CD8 (Dynabeads, Deutsche Dynal).

Channel activation. To measure channel activation, test depolarizations between –107 and –67 mV were applied in steps of 5 mV every 5 s (DRG) or between –127 and 13 mV in steps of 10 mV every 3 s (ND7/23 cells). The voltage dependence of channel activation (Figs. 4 and 5), based on mean current densities, was estimated with the following formalism:

$$\frac{I(V)}{C} = \Gamma(V - E_{\text{rev}})P_{\text{open}}(V)$$

$$P_{\text{open}}(V) = \frac{1 - P}{1 + e^{-(V - V_m)/k_m}} + \frac{P}{1 + e^{-(V - V_{\text{mp}})/k_{\text{mp}}}}$$

where C is the cell capacitance, Γ is the conductance density and E_{rev} is the reversal potential. Open probabilities (P_{open}) were described with a double Boltzmann function to account for the presence of wild-type ($1 - P$) and mutant (P) Na_v1.9 channels in DRG neurons from heterozygous knock-in mice. P , the fraction of mutant channels, was set to zero for the analysis of wild-type channels (Figs. 4b, mouse Na_v1.9 and 5b, human Na_v1.9) and was set to one for the mutant channels (Figs. 4b, mouse Na_v1.9 Leu799Pro and 5b, human Na_v1.9 Leu811Pro). V_m and V_{mp} are the half-maximal activation voltages characterizing the activation of wild-type and mutant Na_v1.9 channels, respectively; k_m and k_{mp} are the associated slope factors. Activation of the mixed channel population in neurons from heterozygous knock-in mice (Fig. 4b, *Scn11a*^{+L799P} genotype) was described with V_m , k_m , V_{mp} and k_{mp} set to the values obtained from fits of wild-type (*Scn11a*^{+/+} genotype) and mutant Na_v1.9 (*Scn11a*^{-L799P} genotype), and P was set to 0.5 assuming an equal contribution of channel variants.

Gating kinetics. Current traces of human Na_v1.9 and Na_v1.9 Leu811Pro channels were analyzed between –37 and 3 mV with a simplified gating model to infer the kinetics of channel activation and inactivation

$$I(t) = I_0 m(t) h(t)$$

$$m(t) = 1 - e^{-(t/\tau_m)}$$

$$h(t) = h_{\infty} + (1 - h_{\infty})e^{-(t/\tau_h)}$$

with the current amplitude I_0 . $m(t)$ and $h(t)$ describe the kinetics of channel activation and inactivation, respectively; τ_m and τ_h are the associated time constants, and h_{∞} characterizes the fraction of non-inactivating current after infinite time. Data for Na_v1.9-L811P were best described when h_{∞} was set to zero.

Steady-state inactivation. Na_v1.9 channels were activated with a first 50-ms test pulse to –67 mV (DRG neurons) or –47 mV (ND7/23 cells) followed by a conditioning interval of 500 ms at voltages ranging from –127 to –57 mV (DRG neurons) or from –127 to –17 mV (ND7/23 cells). Peak currents of channels that were not inactivated were measured in a subsequent 50-ms test pulse. The repetition interval was 10 s for DRG neurons and 20 s for ND7/23 cells. The current after conditioning ($I_{500\text{ms}}$) normalized to the control current (I_0) was described with the following Boltzmann formalism:

$$\frac{I_{500\text{ms}}(V)}{I_0} = h_{\max} - (h_{\max} - h_{\min}) \left(\frac{1 - P}{1 + e^{-(V - V_h)/k_h}} + \frac{P}{1 + e^{-(V - V_{\text{hp}})/k_{\text{hp}}}} \right)$$

with h_{\min} and h_{\max} being the maximal and minimal channel availability, respectively, and the half-maximal inactivation voltages V_h and V_{hp} characterizing the inactivation of wild-type and mutant channels, respectively; k_h and k_{hp} are the corresponding slope factors. P , the fraction of mutant channels, was set to zero to analyze inactivation of wild-type channels (Figs. 4f, mouse Na_v1.9 and 5f, human Na_v1.9) and was set to one for the mutant (Figs. 4f, mouse Na_v1.9 Leu799Pro and 5f, human Leu811Pro). In neurons from heterozygous knock-in mice (Fig. 4f, *Scn11a*^{+L799P} genotype), P was estimated by describing the inactivation with V_h , k_h , V_{hp} and k_{hp} set to the values obtained from fits of wild-type (*Scn11a*^{+/+} genotype) and mutant Na_v1.9 (*Scn11a*^{-L799P} genotype).

Channel deactivation. Channels were activated with a 25-ms depolarization to –67 mV (DRG neurons) or –47 mV (ND7/23 cells) followed by a 150-ms repolarization period at voltages ranging from –117 to –77 mV in steps of 5 mV with a repetition interval of 10 s. The current decay during the repolarization period was fitted according to

$$I(t) = I_0 - (I_0 - I_{\infty}) \left((1 - P)(1 - e^{-t/\tau_{\text{fast}}}) + P(1 - e^{-t/\tau_{\text{slow}}}) \right)$$

where I_0 is the maximal current amplitude and I_{∞} is the current remaining after infinite time. τ_{fast} and τ_{slow} are the deactivation time constants of wild-type and mutant Na_v1.9 channels, respectively. The fraction of slowly deactivating mutant channels, P , was set to zero to analyze deactivation of wild-type channels (Figs. 4d, mouse Na_v1.9 and 5d, human Na_v1.9) and was set to zero for mutant channels (Figs. 4d, mouse Na_v1.9 Leu799Pro and 5d, human Na_v1.9 Leu811Pro). Deactivation of tail currents in DRG neurons from heterozygous knock-in mice (Fig. 4d, *Scn11a*^{+L799P} genotype) was readily described with τ_{fast} and τ_{slow} set to the values obtained from fits of wild-type (*Scn11a*^{+/+} genotype) and mutant (*Scn11a*^{-L799P} genotype) Na_v1.9, yielding P .

The voltage dependence of activation and deactivation time constants was described with

$$\tau(V) = \tau_0 + \frac{1}{\alpha_0 \left(e^{\frac{(V - V_0)q\delta}{kT}} + e^{\frac{-(V - V_0)q(1 - \delta)}{kT}} \right)}$$

where τ_0 is the voltage-independent limiting speed of deactivation, α_0 is the rate at the equilibrium voltage V_0 and kT is the thermal energy. q is the total gating charge transfer, and δ is the symmetry factor specifying the relative

position of the activated state within the electric field. Deactivation time constants for wild-type (*Scn11a*^{+/+} genotype) and mutant (*Scn11a*^{-/L799P} genotype) Na_v1.9 in DRG neurons were described with q , τ_0 and α_0 constrained to be identical; δ was set to 0.5, and V_0 was fixed to 0 for wild-type channels, yielding an estimate of the mutation-induced shift in the voltage dependence of deactivation. Fast and slow deactivation components of channels from *Scn11a*^{+/L799P} mice were analyzed using the same approach with q set to the value obtained for channels from *Scn11a*^{+/+} and *Scn11a*^{-/L799P} mice. Activation and deactivation time constants of human wild-type and mutant channels were subjected to a global fit with q , τ_0 , α_0 and δ constrained to be identical.

Recording of mEPSCs. Spinal cord slices (350 μ m) were prepared from 6- to 10-d-old mice as described²⁷ and were equilibrated in artificial cerebrospinal fluid (aCSF; 120 mM NaCl, 3 mM KCl, 1.3 mM MgSO₄, 1.25 mM NaH₂PO₄, 2.5 mM CaCl₂, 10 mM glucose and 25 mM NaHCO₃ gassed with 95% O₂/5% CO₂, pH 7.3) at room temperature for at least 1 h. Spinal cord slices were placed in a recording chamber mounted on an upright microscope (BX51WI, Olympus) and continuously superfused with oxygenated aCSF. Neurons from the substantia gelatinosa of posterior horns were selected for whole-cell patch-clamp recordings using a Multiclamp 700B amplifier and pClamp 10.2 software (Axon Instruments). mEPSCs were recorded as described previously⁴⁴ at a holding potential of -70 mV for at least 5 min. mEPSCs were isolated by adding tetrodotoxin (0.5 μ M; Tocris) and bicuculline methiodide (20 μ M; Biomol) to block action potential-induced glutamate release and GABA_A receptor-mediated miniature inhibitory postsynaptic currents, respectively. The pipette solution contained 120 mM CsMeSO₄,

17.5 mM CsCl, 10 mM HEPES, 5 mM BAPTA, 2 mM Mg-ATP, 0.5 mM Na-GTP and 10 mM QX-314, pH 7.3, adjusted with CsOH. Currents were identified as EPSC when the rise time was faster than the decay time; EPSC amplitudes, inter-event intervals and average event frequencies were determined.

Data were analyzed with FitMaster (HEKA Elektronik), IgorPro (WaveMetrics) and ClampFit (Axon Instruments) software. Data are presented as mean \pm s.e.m. Statistical comparisons of two groups of data were made using the two-sided Student's *t* test; *P* values are given explicitly.

38. Schröder, J.M., Hoheneck, M., Weis, J. & Deist, H. Ethylene oxide polyneuropathy: clinical follow-up study with morphometric and electron microscopic findings in a sural nerve biopsy. *J. Neurol.* **232**, 83–90 (1985).
39. Schwenk, F., Baron, U. & Rajewsky, K. A *cre*-transgenic mouse strain for the ubiquitous deletion of *loxP*-flanked gene segments including deletion in germ cells. *Nucleic Acids Res.* **23**, 5080–5081 (1995).
40. Ebbinghaus, M. *et al.* The anti-inflammatory effects of sympathectomy in murine antigen-induced arthritis are associated with a reduction of Th1 and Th17 responses. *Ann. Rheum. Dis.* **71**, 253–261 (2012).
41. Richter, F. *et al.* Interleukin-17 sensitizes joint nociceptors to mechanical stimuli and contributes to arthritic pain through neuronal interleukin-17 receptors in rodents. *Arthritis Rheum.* **64**, 4125–4134 (2012).
42. Blum, R., Kafitz, K.W. & Konnerth, A. Neurotrophin-evoked depolarization requires the sodium channel Na_v1.9. *Nature* **419**, 687–693 (2002).
43. Dib-Hajj, S.D. *et al.* Transfection of rat or mouse neurons by biolistics or electroporation. *Nat. Protoc.* **4**, 1118–1126 (2009).
44. Sinning, A. *et al.* Synaptic glutamate release is modulated by the Na⁺-driven Cl⁻/HCO₃⁻ exchanger Slc4a8. *J. Neurosci.* **31**, 7300–7311 (2011).